Journal of Applied Fluid Mechanics, Vol. 17, No. 3, pp. 697-712, 2024.
Available online at www.jafmonline.net, ISSN 1735-3572, EISSN 1735-3645.
https://doi.org/10.47176/jafm.17.3.2052

Effect of GNP/Ni-TiO_2 Nanocomposite Coated Copper Surfaces Fabricated by Electro Chemical Deposition under Nucleate Pool Boiling Regime: A Comprehensive Experimental Study

B. Shil[1], D. Sen[2†], A. K. Das[1], P. Sen[1] and S. Kalita[2]

[1]*Department of Mechanical Engineering, National Institute of Technology Agartala, Tripura-799046, India*
[2]*Department of Mechanical Engineering, National Institute of Technology Arunachal Pradesh, Jote-791113, India*

†Corresponding Author Email: dipak@nitap.ac.in

ABSTRACT

Current study presents an experimental analysis of nucleate pool boiling on the GNP/Ni-TiO_2 (GNP-graphene nano particle) nano-composite coated copper surfaces. In order to produce the microporous surfaces, a two-step electro-deposition process is used. This deposition results in the formation of a modified surface structure, and various surface morphological characteristics of this modified structure, like wettability, roughness and surface structure are studied. The results reveal an improvement in CHF (critical heat flux) and BHTC (boiling heat transfer coefficient) in case of GNP/Ni-TiO_2 coated surfaces. The main elements influencing the improved heat transfer of the GNP/Ni-TiO_2nano-composite coating are its increased wettability, roughness, and high thermal conductivity. The SNCCC (superhydrophilic nano-composite coated copper) surfaces have the maximum BHTC of 97.52 (kW/m^2K) and CHF of 2043 (kW/m^2), which are 93% and 88% higher than the base Cu surfaces respectively. Here, it is analysed how the performance of SNCCC surfaces are enhanced by the impact of different parameters, like the roughness of the surface and wettability. The bubble characteristics at the time of boiling is noticed using a high-speed camera, and several factors such as nucleation site density, bubble departure diameter, and bubble emission frequency are statistically studied for SNCCC surfaces.

Article History

Received June 7, 2023
Revised November 1, 2023
Accepted November 4, 2023
Available online January 1, 2024

Keywords:

BHTC
Bubble dynamics
CHF
Electrochemical deposition
Superhydrophilic surface

1. INTRODUCTION

There are various industrial applications for boiling heat transfer, including heat exchangers, refrigeration and air-conditioning, power generation sector, space devices, microelectronics chip devices, refining of petroleum etc., (Al-Chaabawi et al., 2023; Shah et al., 2023; Wang et al., 2023a, b), which require very quick dissipation of heat from a constrained area. Improvement in the performance of pool boiling heat transfer is crucial for increasing the effectiveness of these industrial applications.

Two important criteria that assess the level of nucleate pool boiling heat transfer performance are the CHF and the BHTC. While critical heat flux is the factor that ensures the system's safety, BHTC is frequently used as a benchmark for the efficiency of heat transfer of any system. Therefore, increasing boiling HTC is crucial for significantly reducing energy consumption (Dai et al., 2019), system size and volume, and the boiling systems become more energy-efficient due to this HTC improvement. High CHF values are preferred in different thermal management applications to prevent issues like burnout and dry-out.

Researchers have recently concentrated on several methods for the modification of boiling surfaces to increase the CHF in nucleate pool boiling. Modifications of surface frequently result in changes to the surface properties like as wettability (Mohammadi et al., 2018; Wang et al., 2018; Yim et al., 2019; Shi et al., 2020) roughness (Kim et al., 2016; Alvariño et al., 2019;

NOMENCLATURE

BHTC	Boiling Heat Transfer Coefficient	T2	thermocouple 2 temperature
CA	Contact Angle	T3	thermocouple 3 temperature
CHF	Critical Heat Flux	T_f	saturation temperature of boiling fluid
C_p	specific heat at constant pressure	T_s	boiling surface temperature
D_d	departure diameter of bubble	x	distance between thermocouple
dT/dx	temperature gradient	y	distance between thermocouple 1 and testing sample
h	coefficient of heat transfer	ΔT	wall superheat
K_{cu}	copper thermal conductivity	λ	latent heat of vaporization
N_a	active nucleation site density	μ	dynamic viscosity
q//	heat flux	ρ	density
R_a	value of average surface roughness	σ	surface tension
T1	thermocouple 1 temperature	ONB	Onset Nucleate Boiling

Arenales et al., 2020) heating orientation (Jun et al., 2016; Chuang et al., 2019) porosity, etc., which have an impact on CHF & BHTC.

There are active and passive processes for boiling heat transfer augmentation approaches. Active mechanisms employ electrostatic fields, ultrasonic vibrations, etc.; nevertheless, their application is typically restricted due to their high energy requirements and intricate design. The most useful` approaches are passive ones since they improve heat transfer while reducing the size of the equipment. The passive method uses a variety of surface modification techniques, such as the creation of different microporous or nanotextured surfaces, fabrication of macrostructures by mechanical machining (ex-grooves and fins) etc. Various surface modification techniques are utilised in passive mechanisms like porous coating, nanotexture, nanowire, micro-channel, pin-fin, nanoparticle deposition etc. (Vemuri & Kim, 2005; Ahn et al., 2006; Kim et al., 2007; Ujereh et al., 2007; Huang et al., 2011; Saelim et al., 2011; Lu et al., 2011; Jun et al., 2013; Tang et al., 2013; Shi et al., 2015; Das et al., 2016; Das et al., 2017a, b; Gupta & Misra, 2018).

As was previously indicated, improving the surface's wettability is essential for enhancing heat transfer performance. The research by Mogra et al. (2021) suggested increasing BHTC for hydrophobic surfaces and CHF for hydrophilic surfaces. According to Shi et al. (2020) the performance of superhydrophilic surfaces is better in medium/high heat flux zones but the performance of superhydrophobic surfaces is well in lower heat flux region.

The analysis of the literature shows that CHF displayed a striking reliance on surface roughness. The CHF increases with the improvement of surface roughness, and this augmentation in CHF is caused by capillary wicking, which provides significant amount of liquid to the hot spots from the surroundings. (Kim et al., 2016). According to research by Kim et al. (2018) even though the BHTC for hydrophobic surfaces was initially high, it considerably reduced as the flux of heat increased, and the CHF for hydrophobic surfaces was significantly lesser than that of hydrophilic surfaces. It is observed from the above literature that the enhancement in the wettability and roughness of the surface augment the performance of nucleate pool boiling.

In the area of surface-controlled occurrences like nucleate pool boiling, surface modification employing coating of nanostructure generates a wide field of inquiry. TiO_2 nanoparticles coated porous structures increase CHF and decrease BHTC, according to Huang et al. (2011). The boiling experiment using a mixed nanofluid of water, SiO_2 and ethylene glycol shows that BHTC improves as nanoparticle diameter decreases. Additionally, BHTC initially enhanced rapidly as nanoparticle concentration increased, but a drop in BHTC was detected in the concentration range of 0.25 to 1.00% (Hu et al., 2017). Applications of various nano-particles also enhance the performance of heat transfer during boiling, which is revealed from the above literature about nano particles.

Because of its greater thermal conductivity, distinctive mechanical characteristics and high transparency, now a day's, there is a lot of interest in graphene. In comparison to pure water, GO nanofluids increase the CHF by roughly 40–200%, according to research by Park et al. (2012). At atmospheric pressure, Mao et al. (2020) accomplished nucleate pool boiling studies on GO nanocoating surfaces with DI. Compared to the bare copper surface, experimental outcomes show improvements of 78% in CHF and 41% in BHTC. For graphene surfaces, Seo et al. (2015) demonstrated high CHF enhancement by using of FC-72 refrigerant as the boiling fluid. The use of graphene nanoparticles from the aforementioned literature is found to improve heat transmission performance in terms of CHF and BHTC enhancement. The CHF and BHTC enhancement were found compared to the uncoated copper surface, according to Gupta and Misra (2019) experimental examination of pool boiling on Cu surfaces electrochemically coated with Cu-TiO_2 composite. Rishi et al. (2018) discovered an improvement in CHF and BHTC by utilizing a surface fabricated by electro-deposition process. Gheitaghy et al. (2016) gained an improvement in CHF and BHTC compared to the uncoated copper surface by utilizing a surface fabricated by electro-deposition and WEDM technology. Gheitaghy

et al. (2018) presented an increase in BHTC and CHF by using electrodeposited microporous surfaces in contrast to the uncoated surface.

A review of the literature reveals that electrochemical deposition approach is a more efficient technology than other ones for creating these microporous surfaces for CHF and BHTC enhancement. The surface fabrication process stated above is relatively simple, controlled, cost-effective, and appropriate for mass production. The literature analysis also reveals that relatively few attempts have been made to create microporous surfaces employing a hybrid technique in order to improve the nucleate pool boiling heat transfer. To the authors' knowledge, no research has been done on the hybrid approach (electro-deposition of GNP and coating of Ni-TiO_2) for creating microporous surfaces to improve pool boiling performance. Thermal management systems with high heat flux must have high CHF and BHTC of the heated surface in order to move a significant amount of heat quickly. These days, nanoparticles of graphene are increasingly relevant for a vast range of engineering fields because of their superior thermal and mechanical characteristics. Because of this, the microporous surfaces in the current study are created utilising a hybrid approach that involves two steps of electrochemical deposition. The first step in making the microporous surface involves the deposition of GNP, and the copper surface coated with GNP/Cu composite is then covered with a Ni-TiO_2 nanocomposite coating. The performance of pool boiling on bare Cu surfaces coated with GNP/Ni-TiO_2 nano-composite is experimentally investigated in this study. The present work additionally examines surface characterisation factors like roughness, wettability and structure of surface and their impacts on the performance of the heat transmission during pool boiling. Here, CHF and BHTC are investigated, and quantitative research is also done on the bubble dynamics of the modified surface.

2. METHODOLOGY

2.1 Surface Preparation

An electrochemical deposition process is used to create four different superhydrophilic nanocomposite-coated copper (SNCCC) surfaces on bare copper for the purpose of evaluating the performance of pool boiling. Prior to starting the electro-deposition process, typical oxides are removed from basic Cu surfaces using sandpaper. Following the elimination of typical oxides, the bare copper surfaces are subjected to 10 minutes of ultrasonic cleaning with each acetone, ethanol, and DI (distilled water). This case involves two steps for surface fabrication. First, a composite coating of GNP/Cu is applied to the cleaned, basic Cu surface. Next, coating of Ni-TiO_2 nano-composite is provided on the copper plate coated with GNP/Cu composite.

2.1.1 GNP/Cu Composite Coating Deposition

The electrochemical deposition of graphene nanoparticles on a bare, cleaned copper surface is done according to Rishi et al. (2019). A copper block acts as the cathode in the cell, and an additional copper test surface

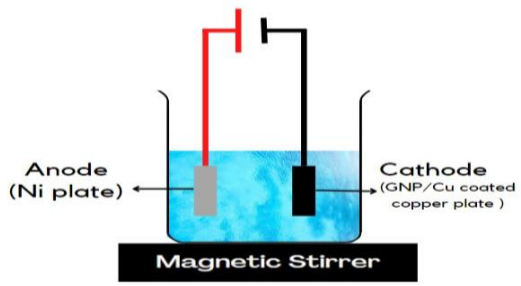

Fig. 1 Deposition (Electrochemical) of Ni-TiO_2 composite

Table 1 Components of electrolyte

Component	Concentration (g/L)
Nickel sulphate hexahydrate ($NiSO_4.6H_2O$)	100
Nickel chloride hexahydrate ($NiCl_2.6H_2O$)	40
Boric acid (H_3BO_3)	25
Sodium dodecyl sulphate ($Na_2SO_410H_2O$)	50
TiO_2 nanoparticle	25 (SNCCC1), 50 (SNCCC 2), 75 (SNCCC 3), 100 (SNCCC4)

performs as the anode. The electrolytic bath's constituents are H_2SO_4 (1.5 M), $CuSO_4$ (0.8 M), GNP with 2% *W/V* (weight/ volume) and 120 mL distilled water. $CuSO_4$ and H_2SO_4 undergo an exothermic chemical reaction. Because of this, the water is added twice, 60 mL earlier than the addition of H_2SO_4 and 60 mL after the addition of H_2SO_4. After that, an ultrasonicator is used to sonicate the electrolyte solution for 45 minutes in order to prevent the nanoparticles from clotting. Throughout the entire electro-deposition process, a Teflon holder is used to keep the cathode and anode 3 mm apart from one another. Throughout the electro-deposition process, a constant current is used to deposit copper along with the GNP. First, in order to advance hydrogen bubbles during the deposition process, 400mA/cm2 current density is applied for 15 seconds. A lower density of current 40 mA/cm^2 is then supplied for the remaining 2500 seconds, strengthening the connection between the depositions of particles. Following the electro-deposition procedure, the electro-deposited copper plate is washed with DI and dried with hot air before moving on to the next phase, the deposition of Ni-TiO2 composite nanoparticles.

2.1.2 Deposition of Ni-Al_2O_3 Composite Coating

This process involves depositing Ni-TiO_2 composite on the copper plate coated with GNP/Cu composite using the method of electrochemical deposition shown in Fig. 1. Table 1 contains information regarding the electrolytic bath's composition (Fawzy et al., 1996). Electrolytic solutions with four different concentrations of TiO_2 nanoparticle (given in table 1) are created for this deposition technique. The anode is a nickel plate, while the cathode is a GNP/Cu-coated copper plate. The

electrolyte's pH is kept at 4 +/- 0.2. By keeping the electrolytic bath at 45 ± 5℃, stirring it constantly at 250 rpm, and using a density of current 60mA/cm^2, the deposition method is continued for 45 minutes (Tey et al., 2015). Following the deposition, the samples are cleaned with DI, and then they are dried by hot air *Pool Boiling Experimental Facility and Method*

We carry out the nucleate pool boiling experiment using DI as the working fluid. A copper block is used to apply heat to the testing surface. The Cu block's bottom has a cartridge heater (400W) installed as the heat source. To reduce heat loss, the copper block has been completely insulated with glass wool. A M-Seal clear RTV silicon sealant is fitted with the prepared SNCCC surface on the top surface of the metallic block. This sealant prevents the penetration of the boiling fluid between the SNCCC surface and metallic block. To increase the efficiency of the heat transfer, highly conductive Omega High temperature and Conductive thermal paste has been used. T_1, T_2, and T_3 are three K-type thermocouples that are placed on copper to measure the temperature of the testing surface. DAS is used to obtain the thermocouple readings. The testing chamber is furnished with a 100W cartridge heater that is coupled to a PID controller, for maintaining the saturation temperature of the working fluid. A constant-temperature water bath condenses the continuously forming vapor bubbles inside the testing chamber, preserving the chamber's constant fluid level. In order to completely eliminate the gases (non-condensable), the testing chamber is initially filled with 200 mL (about) of DI water that is continuously heated at saturation temperature for a time being (3–4 hours). The 400 W cartridge heater is then used to apply a heat flux to the SNCCC surface. It takes the system 3–4 hours to attain a steady state after the initial heat flux is supplied. The system is said to be in a steady state when the temperature changes by 0.2 C per minute. The readings of each thermocouple temperature are recorded once the first heat flux has stabilized. Then, small enhancement in the flux of heat to the SNCCC surface occurs. The time it takes for the system to achieve steady state after the second heat flux is introduced is close to 40–45 minutes. Temperatures of the thermocouples are measured when the boiling system is in steady condition. Up until the boiling system reaches the CHF, the flux of heat that is provided to it is steadily enhanced. The system rapidly changes thermocouple temperatures when the CHF is achieved, and power to the SNCCC surface is then switched off as a result.

Equation 1 estimates the heat flux (q'') of the SNCCC surface using the Fourier Law of Heat Conduction, where dT/dx is the temperature gradient of the copper block close to the boiling surface. The temperature gradient is determined using a three point Taylor series approximation and is represented in equation 2. It is assumed that the copper block's sides are all adiabatic when calculating the temperature gradient.

$$q'' = -k_{cu}\frac{dT}{dx} \tag{1}$$

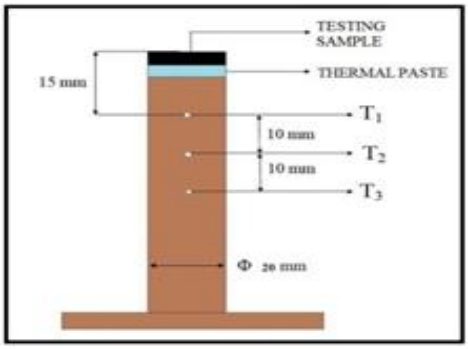

Fig. 2 Position of thermocouples with test sample

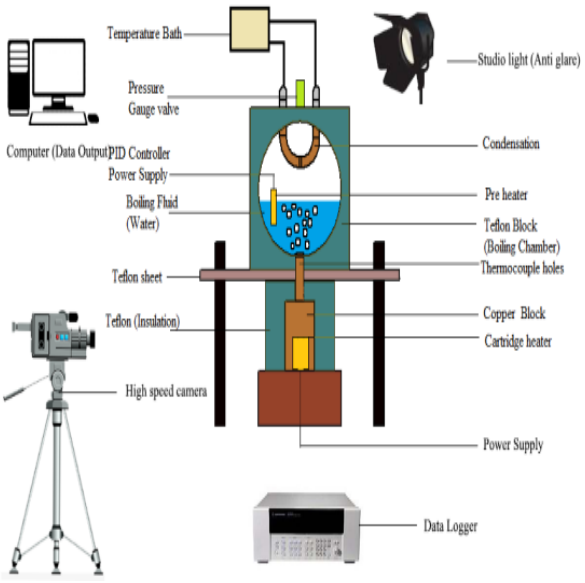

Fig. 3 Schemic diagram of experimental pool boiling set up

$$\frac{dT}{dx} = \frac{3T_1 - 4T_2 + T_3}{2x} \tag{2}$$

As a result, equation 1 yields the heat flow, and equation 3 is employed to determine the boiling surface temperature (T_s).

$$T_s = T_1 - \frac{q''.y}{k_{cu}} \tag{3}$$

Lastly, equation 4 is used to calculate the BHTC (h) of SNCCC surfaces.

$$h = \frac{q''}{T_s - T_f} \tag{4}$$

2.3 Error Analysis

Analysis of each parameter's uncertainty is crucial because the parameters are derived experimentally. Calculating the level of uncertainty associated with each parameter is done using the Kline and McClintock approach (Namaraa et al., 2019). Equations 5, 6, and 7 are utilized to calculate the uncertainty in CHF (q''), BHTC (h), and boiling surface temperature (T_s).

$$\frac{\omega_q}{q} = \left[\left(\frac{3\omega_{T_1}}{3T_1 - 4T_2 + T_3}\right)^2 + \left(\frac{4\omega_{T_2}}{3T_1 - 4T_2 + T_3}\right)^2 + \left(\frac{\omega_{T_3}}{3T_1 - 4T_2 + T_3}\right)^2 + \left(\frac{\omega_x}{x}\right)^2\right]^{\frac{1}{2}} \quad (5)$$

$$\frac{\omega_{T_s}}{T} = \left[\left(\frac{K_{cu}\omega_{T_1}}{K_{cu}T_1 - q.y}\right)^2 + \left(\frac{y.\omega_q}{K_{cu}T_1 - q.y}\right)^2 + \left(\frac{q.\omega_y}{K_{cu}T_1 - q.y}\right)^2\right]^{\frac{1}{2}} \quad (6)$$

$$\frac{\omega_h}{h} = \left[\left(\frac{\omega_q}{q}\right)^2 + \left(\frac{\omega_{T_s}}{T_s - T_f}\right)^2\right]^{\frac{1}{2}} \quad (7)$$

The uncertainty in measuring the separation between the testing surface and the first thermocouple (T_1) is given byω_y and the gap between the thermocouples is denoted by ω_x in the above equations. Repeated physical measurements reveal that those distances are measured with an inaccuracy of 5.2%. It is found that the heat fluxes have maximum uncertainty of 12.1%. Again, the measurement uncertainty for temperatures is set at 1.3%. Similarly, for the T_s and the h, uncertainty is 8.8% and 10.8%, respectively.

3. EXPERIMENTAL RESULTS AND DISCUSSION

3.1 Characterisation of SNCCC Surface

To analyse the morphology of surface, SEM is utilised. Figure 4 depicts different magnifications of the graphene and TiO_2 electrodeposited porous copper morphologies. The deposited structure is the outcome of the competition between the movement of hydrogen bubbles off the surface and the deposition of metal on the surface (Patil et al., 2014). The interaction of hydrodynamic and electrochemical characteristics determines the result of this competition. (Nikolic, 2010). The Ni-TiO_2 nanocomposite coating shows algae floral-type structures, which are seen in Fig. 4(a-d). Numerous cavities and pores are noticed in the FESEM pictures of GNP/Ni-TiO_2 coated microporous surfaces. During the boiling process, these cavities serve as good active zones for the creation of bubbles. The nickel and graphene matrix in picture 4(a-d) has white agglomerated nanoparticles implanted. With the increase of amount of TiO_2 in the electrolyte bath, the morphology of surface of the GNP/Ni-TiO_2 coating significantly changes. The nano-composite coated surfaces fabricated at lesser TiO_2 concentrations are made of grains of globular size. But when the amount of TiO_2 in the electrolyte bath rises, the size of pore alters to become bigger and cruder, assembling more particles, as shown in the images 4(e-h). Numerous micro pores are produced as the concentration of TiO_2 rises. Cauliflower-like structure

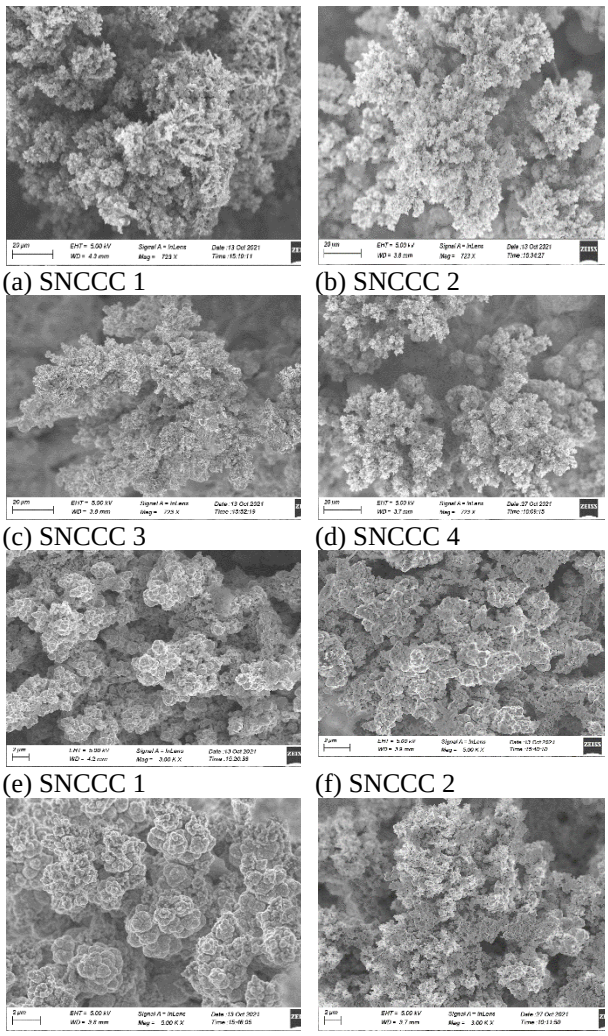

(a) SNCCC 1 (b) SNCCC 2 (c) SNCCC 3 (d) SNCCC 4 (e) SNCCC 1 (f) SNCCC 2 (g) SNCCC 3 (h) SNCCC 4

Fig. 4 SEM images for all SNCCC surfaces. 723 X (a-d) and 15.00 K X(e-h) for SNCCC surfaces.

is also observed when the TiO_2 concentration rises (figure 4-g).

The curves of the roughness for SNCCC surfaces created by changing the TiO_2 concentration in an electrolytic bath are shown in Fig. 5. The R_a (roughness) of each SNCCC surface and bare copper is measured using an optical surface profiler. The results show that SNCCC surfaces have greater R_a values than the uncoated copper surface. Additionally, it has been found that the SNCCC surfaces' roughness changes with the amount of TiO_2 in the electrolyte bath.

The EDX spectra of each SNCCC surface are shown in Fig. 6. EDX is utilised to inspect the composite on the SNCCC surface. These spectra show the presence of Ni, Ti, and C on the surface of the SNCCC as well as a prominent apex of oxygen, which points to the presence of oxides. This demonstrates that there is a layer of Ni-TiO_2 on the SNCCC surface.

Figure 6: EDX (energy dispersive X-ray) analysis for nano-composite coated (SNCCC) surfaces.

The nucleate pool boiling performance is remarkably impacted by the surface's wettability. The SNCCC surfaces' wettability is investigated via contact angle (CA)

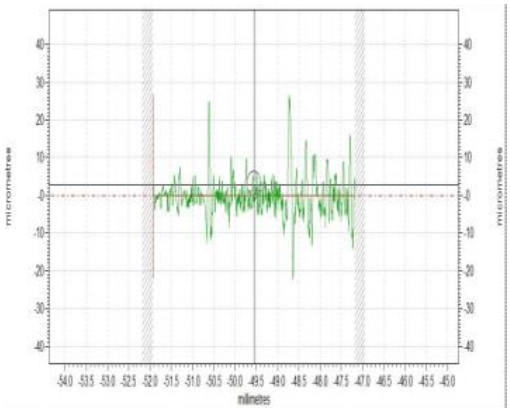

(a) SNCCC 1

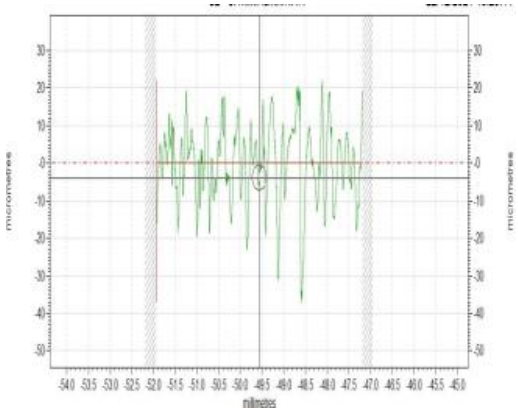

(b) SNCCC2

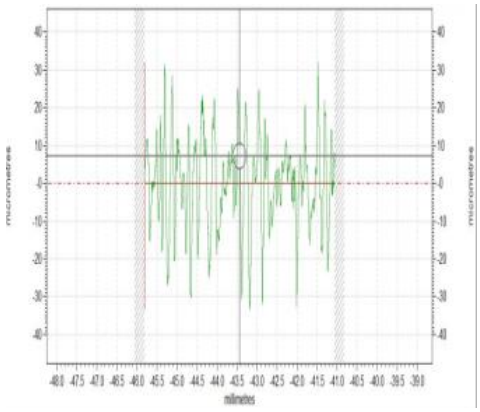

(c) SNCCC 3

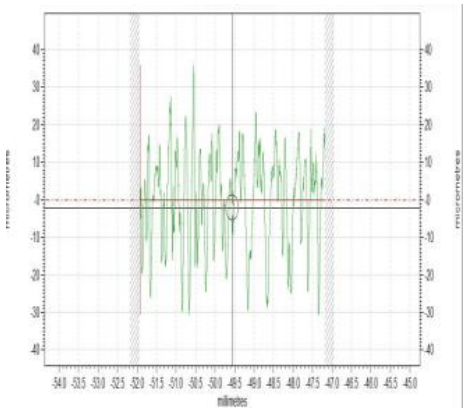

(d) SNCCC 4

Fig. 5 Graph of R_a value of SNCCC surfaces

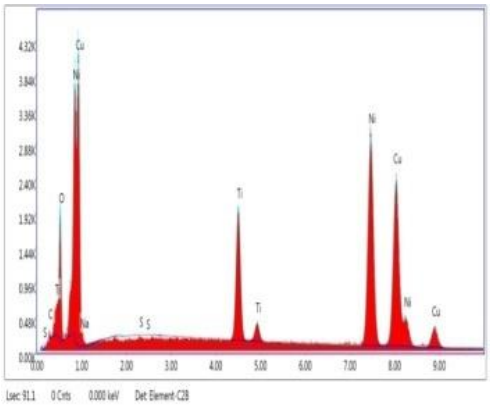

(a) SNCCC1

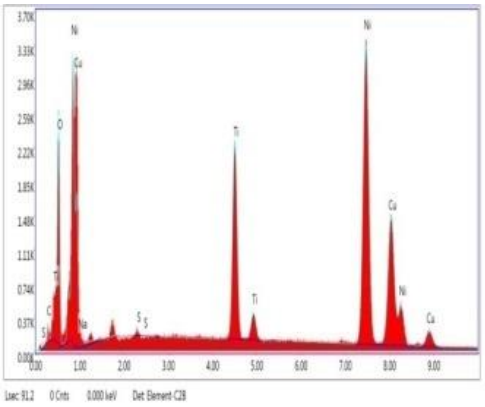

(b) SNCCC 2

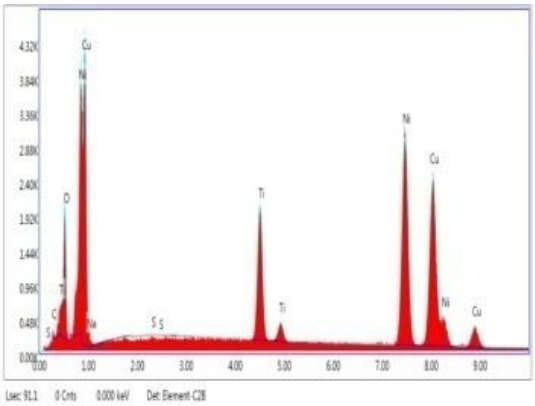

(c) SNCCC 3

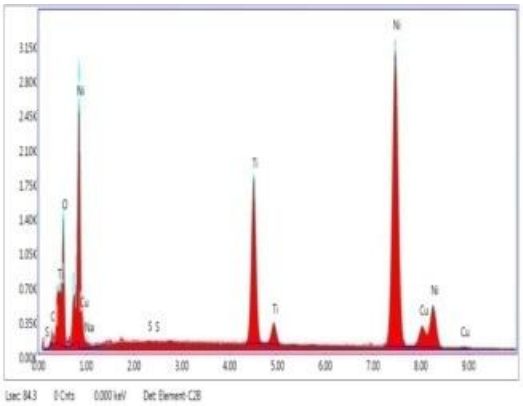

(d) SNCCC4

Fig. 6 EDX for SNCCC surfaces

Table 2 Roughness (R_a) and CA value with CHF & BHTC.

Surface	R_a value (μm)	CA(deg.)	CHF(kW/m^2)	BHTC(kW/m^{2}K)
Bare Cu	0.40	79	1087.4	50.57
SNCCC 1	3.65	21	1905	80.24
SNCCC 2	5.98	18	1944	86.51
SNCCC 3	6.88	14	1997	94.06
SNCCC 4	7.01	12	2043	97.52

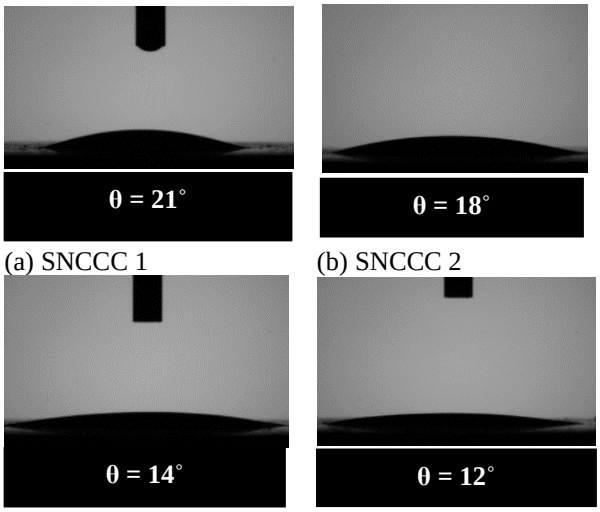

(a) SNCCC 1 (b) SNCCC 2

(c) SNCCC 3 (d) SNCCC 4

Fig. 7 CA (contact angle-sessile drop method) images of nano composite coated (SNCCC) surfaces

measurement. All surfaces under consideration had their CAs assessed with the use of sessile drop method. It is the most straightforward and widely employed strategy. Figure 7 depicts the pictures of contact angle of SNCCC surfaces and Table 2 displays the numerical values. All of the constructed nano composite structured surfaces are found to be superhydrophilic by nature. As the concentration of TiO_2 in the electrolyte rises, it is seen that the CA of SNCCC surfaces reduces, enhancing the surfaces' hydrophilicity.

3.2 Experimental Setup Validation

Verification of the current result on Bare Cu is necessary for authentication of the experimental set up shown in Fig. 2. For this purpose, the boiling curve of the bare Cu is compared with various published literatures (Das et al., 2007; Mori & Okuyama, 2009; Cooke & Kandlikar, 2012; Gheitaghy et al., 2016) and well-known Rohsenow correlation (Rohsenow, 1952) as shown in Eq. (8). The comparative evaluation of the outcomes is represented in Fig. 8. The findings of theoretical and experimental studies show good precision. The Rohsenow correlation is given below:

$$h = \mu_L . h_{lv} . [\frac{g.(\rho_L - \rho_V)}{\sigma}]^{0.5} . (\frac{C_p}{C_{sf} . h_{lv} . Pr})^3 . (T_s - T_f)^2 \quad (8)$$

Surface tension is σ, viscosity is μ, gravitational acceleration is g, vaporisation latent heat is h_{lv}, liquid density is ρ_L, vapour density is ρ_V, Prandtl number is Pr and C_{sf} is 0.0165 in the above equation.

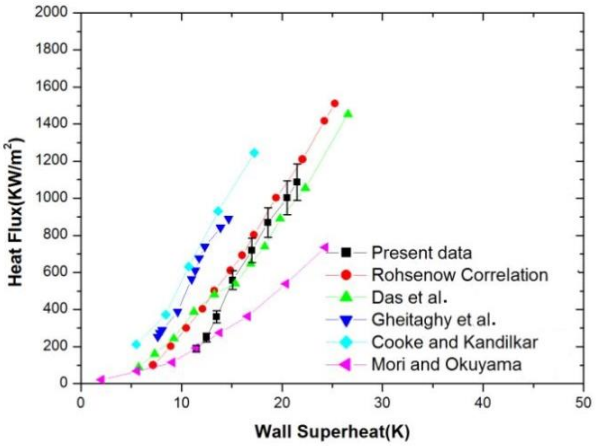

Fig. 8 Validation of experimental arrangement with earlier published literatures

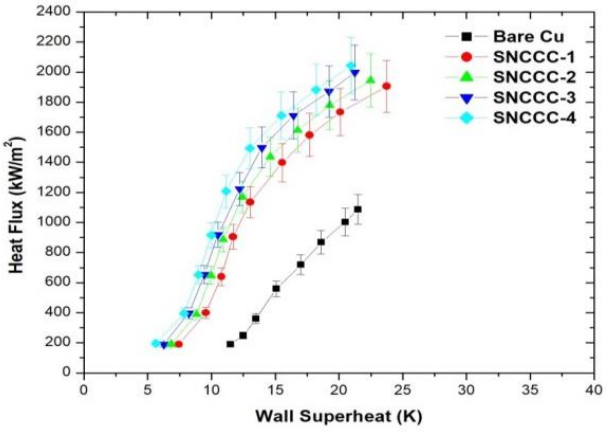

Fig. 9 Boiling curves for bare Cu and prepared surfaces

3.3 Pool Boiling Results

Figure 9 displays the pool boiling curve for all surfaces. For bare Cu surface, the CHF value is 1087.4 kW/m^2. This CHF value matches the CHF value determined by using Zuber's correlation (Fang & Dong, 2016). All of these SNCCC surfaces exhibit greater CHF values than the surface of bare Cu. The maximum CHF value for the SNCCC surfaces (SNCCC 4) is 2043 kW/m^2 with a roughness of 7.01 mm and CA 12^0, while the minimum value (SNCCC 1) is 1905 kW/m^2 with a roughness of 3.65 mm and CA 21^0. Due to the deposition of nano particles on the SNCCC surface, the wettability, roughness and capillary wicking effect of this surface is enhanced and this improvement leads to increase CHF. Table 2 displays the values for the critical heat flux, CA,

and roughness for all surfaces. More amounts of cavities and pores are present on all the nano-composite-covered (SNCCC) surfaces than on uncoated Cu surface, as the SNCCC surfaces have more R_a compare to the bare Cu surface. The ability of a surface to disseminate liquid through capillary wicking is significantly impacted by the presence of nanopores and cavities. Capillary wicking causes the nearby liquid to be pulled into the dry area, which slows the creation of dry spots and raises the CHF on the surface that has been roughened. Surface roughness increased the quantity of capillary wicking, which increased CHF. All of these SNCCC surfaces have a superhydrophilic character, and the results show the augmentation in CHF with the improvement of roughness and wettability. In contrast to the surface of basic Cu, the SNCCC surfaces reach the CHF threshold at a low wall superheat temperature (ΔT). The greater thermal conductivity of graphene contributes to the SNCCC's ability to achieve less ΔT compare to the uncoated copper surface. On the bare surface, a liquid supply is provided by a pressure head (gravitational). The nanopores/cavities found on SNCCC surfaces produce an extra gradient of capillary pressure. This additional pressure gradient helps to flow more amount of liquid to the hot patches from the neighboring sides. The ability of surfaces (covered with nanocomposites) to permit liquid to wick by capillary action, is a significant characteristic of such surfaces. In comparison to bare Cu surfaces, nanocomposite-coated (SNCCC) surfaces have higher CHF values because more fluid flows by capillary action. Results indicate that the CHF is improved with the enhancement of the wettability and capillary wicking of the SNCCC surfaces

All GNP/Ni-TiO_2 coated surfaces have a greater BHTC than bare copper surfaces. Figure 10 depicts how boiling heat transfer coefficient and heat flux are related. The boiling heat transfer coefficient of basic Cu surface is 50.57 kW/m^{2}K, while SNCCC 4 has the highest boiling heat transfer coefficient of all the SNCCC surfaces, measuring 97.52 kW/m^{2}K. The SNCCC1 has the lowest BHTC value of all the SNCCC surfaces, with 80.24 kW/m^{2}K. Table 2 displays the BHTC values for each surface. Results indicate that the improvement of wettability and roughness increases the BHTC for superhydrophilic surfaces (SNCCC surface). A surface coating would improve the R_a and porosity. The nano-composite coating contains more pits and cavities which have a significant influence on bubble formation sites, leads to improvements in performance of boiling. The ability of the liquid to wick through the cavities/pits exist in the nano-composite coating could affect the ΔT during boiling. Therefore, the SNCCC surfaces have higher boiling heat transfer coefficient in comparison with the basic Cu surface, and SNCCC 4 has the maximum BHTC. By allowing the majority of heat to travel through it, the thinner liquid micro-layer that forms beneath the bubble on SNCCC surfaces, aids in increasing boiling heat transmission performance (Phan et al., 2009). Because the cavities in the SNCCC surface feed greater amount liquid to the dry patches than the uncoated Cu surface does, the SNCCC surfaces have less ΔT in comparison with the uncoated copper surface. In comparison with the base Cu surface, the SNCCC surfaces approach the CHF threshold

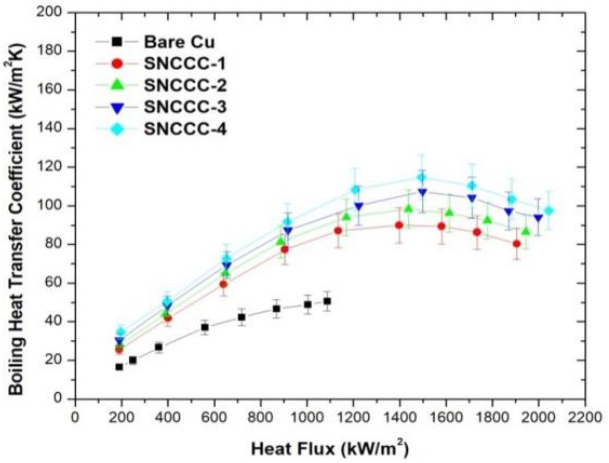

Fig. 10 Heat flux Vs BHTC for bare Cu and prepared surfaces

at a less ΔT. A greater BHTC is indicated by critical heat flux at min. wall superheat (ΔT) (Saeidi & Alemrajabi, 2013). The CHF phenomenon rapidly manifests due to the influence of local heat flux and dry patches. The surface that has the highest CHF with min. wall superheat (ΔT) is therefore considered to be the best surface. According to this analysis, the SNCCC 4 is the most effective since it generates the maximum CHF with the lowest ΔT. Numerous parameters, such as a greater capillary pressure gradient, more active nucleation sites, increased surface area, etc., have a considerable influence on the improvement of performance of heat transfer via nucleate pool boiling. Increased SNCCC surface roughness results in a huge amount of N_a (active bubble sites) that are necessary for the generation of bubbles during boiling, which improves heat transfer performance during boiling.

The CA is utilized to measure the surface wettability and it has an incredible impact on boiling heat transmission process. Micro/nanostructures induce more fluids to spread via capillary wicking, which significantly increases CHF. Table 2 compares the static CA of the surfaces to demonstrate the effect of GNP/Ni-TiO_2 coating on wettability. According to Table 2, all SNCCC surfaces are superhydrophilic by nature and have greater wettability than an uncoated copper surface. The dynamics of the bubbles have an impact on how well heat is transferred during boiling. Smaller bubbles are created and the releasing time of bubble is reduced for all SNCCC surfaces. Due to this, the rate of bubble formation rises, and the nanocomposite coated surfaces' ability to transmit heat during boiling is also improved.

The roughness of the surface is another crucial component that has a significant influence on the performance of boiling. The creation of a large number of holes and cavities contributed to SNCCC surfaces having higher surface roughness values. This holes and cavities act as the locations where bubbles are created. Therefore, the nucleation site density and BHTC are frequently greater in more rough surfaces. The values of each heated surface's roughness are shown in Table 2. The pool boiling performance results demonstrate that the CHF value improves as the R_a increases and Chu et al. also observed

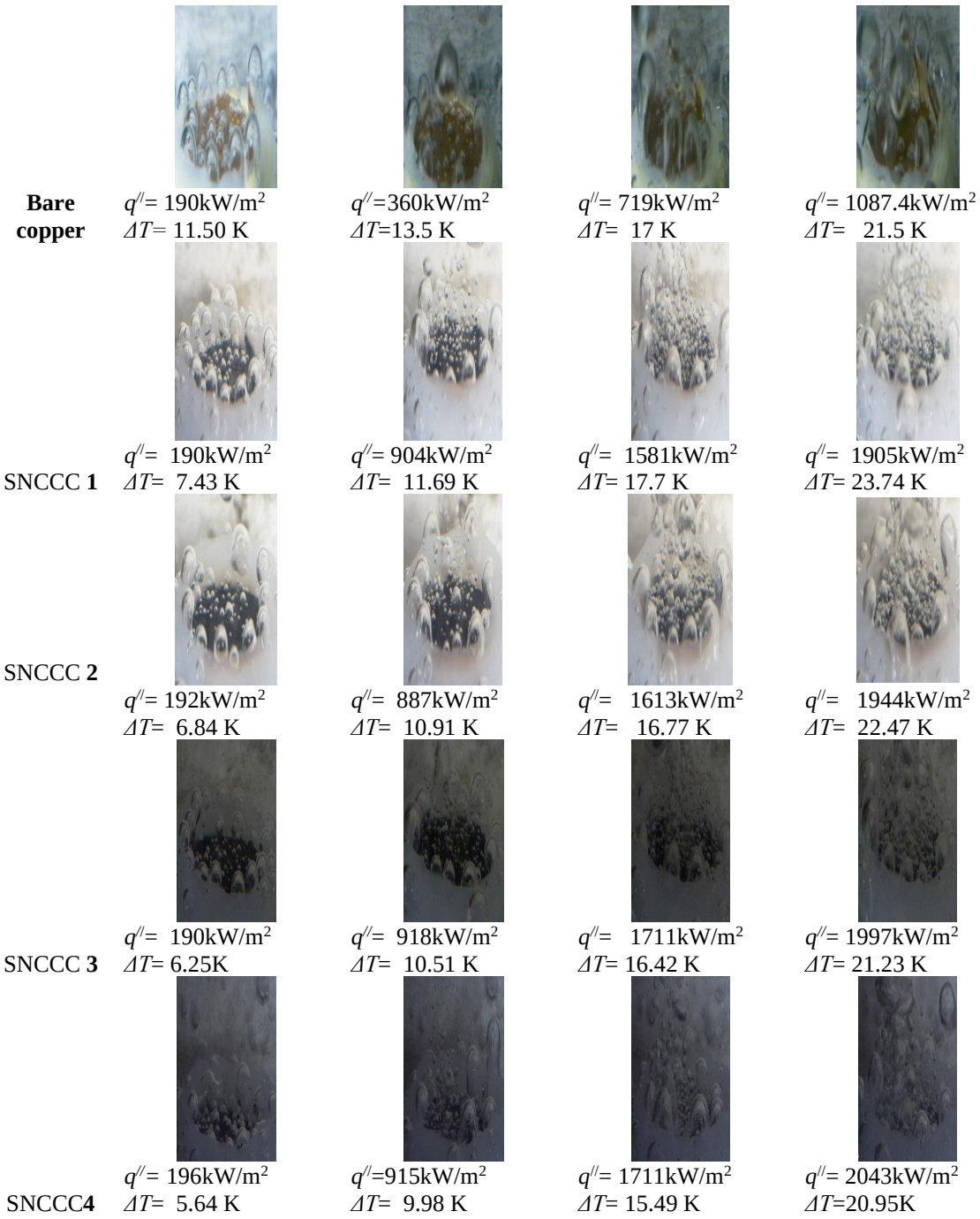

Fig. 11 Bubble dynamics visualization at various heat fluxes for prepared surfaces

same type of trend (Chu et al., 2012). The surface with roughness of 11.76 μm and GNP/Ni-TiO_2 coating (SNCCC4) shows the greatest improvement in CHF and BHTC. The combined effects of surface roughness and cavity creation have resulted in a considerable amount of bubble formation sites, which account for the increase in CHF and BHTC.

3.4 Bubble Dynamics

The study of bubble dynamics which is a part of fluid dynamics, analyze the dynamics (characteristics) of the bubble (i.e gas). Any motion of the fluid during pool boiling is because of the natural convection currents and the movement of bubble is happened due to the effect of buoyancy force. The difference of temperature between the surrounding liquid and the vapour inside a bubble provides the necessary driving force (i.e buoyancy force) for the transmission of the heat between the two phases. Figure 11 shows the dynamics of the bubble as observed by a high-speed camera (Phantom VEO-410). Figure 11 shows bubbles visually for all heated surfaces at varied heat fluxes.

3.4.1 Active Bubble Site Density

The result of the division of total number of active bubble sites by surface area is taken to calculate the active bubble site density (N_a). Some active nucleation sites have been observed to infrequently become inactive, and some inactive heated surface locations have unexpectedly begun to generate bubbles. Moreover, every nucleation sites

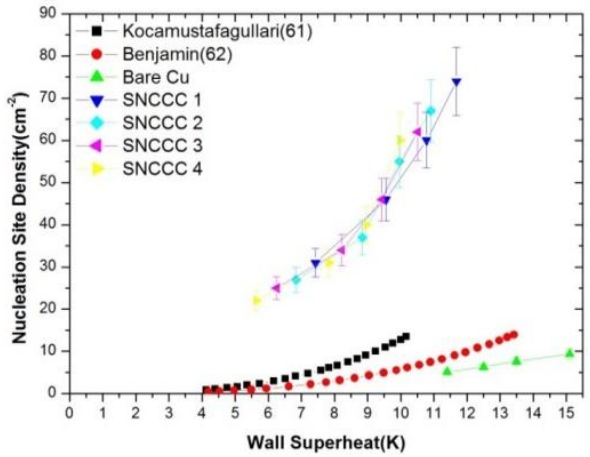

Fig. 12 Nucleation site variation with wall superheat

appear to operate separately from one another. At the region of lower flux of heat, tiny bubbles form on the SNCCC surface without contacting one another. But, a huge number of bubbles appeared on the SNCCC surface with the augmentation of heat flux. These bubbles instantly merged when they made contact with one another. This makes it challenging to see the dynamics of bubble close to the CHF region. As a result, we computed the N_a at the zone of lower heat flux. The N_a variation for all heated surfaces is shown in Fig. 12. Figure 12 illustrates how this N_a value depends on the wall superheat. The value of N_a increases for all the considered surfaces, as seen in Fig. 12, as wall superheat (ΔT) increases. Furthermore, it is observed that the wall superheat (ΔT) required for the formation of the first bubble on the SNCCC surface is smaller than it is for the uncoated Cu surface. This suggests that as compared to the bare Cu surface, the SNCCC surfaces exhibit higher BHTC (Yeom et al., 2015). The SNCCC surfaces contain huge amount of micro-pits and cavities on porous nano-coated surfaces, which trap the vapour and provide a large number of bubble sites for bubble generation. Therefore the N_a of SNCCC surfaces is substantially higher than that of bare Cu surfaces. At the low wall superheat region it is observed that, SNCCC 4 has the lowest nucleation sites and SNCCC1 has the highest sites for the nucleation of the bubbles among the SNCCC surfaces. This is because, with the improvement of surface wettability, the N_a reduces in the case of SNCCC surfaces (Wang & Dhir 1993). However, Fig. 11 shows that the N_a of SNCCC 4 and SNCCC 3 increases extremely significantly with the development of wall superheat. This enhancement in N_a is due to more no bubble sites that were dormant in regions of lower heat flux becoming active in regions of higher heat flux. As a result, the boiling performance of these two surfaces (SNCCC 4 and SNCCC 3) is greatly improved in terms of heat transmission. A modest drop in BHTC is accompanied by a large drop in N_a. As a result, when the surface gets wetter, the BHTC enhances more (Wang & Dhir 1993). When compared to the uncoated Cu surface, ONB for all SNCCC surfaces starts at a relatively lower ΔT, as shown in Fig. 11. For all the SNCCC surfaces, a greater N_a is indicated by the ONB's beginning at a low ΔT. The SNCCC surfaces have higher CHF than bare copper surfaces because *Na* has been increased.

Any surface's nucleation site density depends on a number of factors. Numerous correlations have been created for the analytical computation of nucleation site density based on this two well-known correlations developed by Benjamin and Balakrishman (1997) and Kocumustafaogullari and Ishii (1983) are provided in equations 10 and 9, respectively. Figure 12 makes it obvious that N_a of the basic Cu surface exhibits a similar pattern to that observed in the correlations stated previously. These two well-known correlations were developed for analyzing N_a of various bare surfaces during nucleate pool boiling at the region of low and moderate heat flux. Figure 12 makes it obvious that N_a of the nano-composite coated (SNCCC) surfaces and the bare Cu surface exhibits a similar pattern to that observed in the correlations stated previously. Figure 12 clearly demonstrates that with the improvement of average wall superheat (ΔT), the N_a value rises for all the SNCCC surfaces and this trend is also present in the two well-known correlations stated above. But in the cases of SNCCC surfaces (especially SNCCC 3 and SNCCC 4), from Fig. 12 it is noticed that there is a sharp increase in N_a with the enhancement of wall superheat (ΔT). This enhancement in N_a is due to more no nucleation sites that were dormant in regions of lower heat flux becoming active in regions of higher heat flux. Since SNCCC surfaces exhibit various modified surface characteristics like roughness, porosity etc. which favour the boiling heat transfer enhancement, it also increases nucleation site density simultaneously. The ONB (onset nucleate boiling) at relatively low wall superheat (ΔT) compare to the nano-composite coated surfaces is seen in the cases of above stated two correlations from Fig. 12.

The correlation of Ishii and Kocamustafaogullari is

$$N_a = \frac{2.157 \times 10^{-7} \rho^{*-3.2} (1 + 0.049\rho^*)^{4.13}}{D_d^2 \left[\frac{4\sigma T_{sat}}{\rho_g \Delta T_{sat} h_{lv} D_d}\right]} \quad (9)$$

Where, $\rho^* = \frac{\rho_l - \rho_v}{\rho_v}$, liquid density is ρ_L , ρ_V is vapour density.

Correlation of Benjamin and Balakrishman is

$$N_a = 218.8 \left(\frac{C_p \mu}{\lambda}\right)^{1.63} \left(\sqrt{\frac{\lambda_l \rho_l C_{\rho l}}{\lambda_w \rho_w C_{\rho w}}}\right) \left[14.5 - 4.5 \left(\frac{R_a P}{\sigma}\right) + 0.4 \left(\frac{R_a P}{\sigma}\right)^2\right]^{-0.4} \Delta T^3 \quad (10)$$

In the above equation μ is dynamic viscosity, the roughness is R_a and P is pressure.

3.4.2 Bubble Departure Diameter (D_d)

After assessing the dia. of bubbles for a little while after the bubbles escaped from the surface, the D_d is determined. The holding force and the lifting force of the bubble maintain equilibrium until the bubble reach to a threshold size. When a bubble expands, the force of

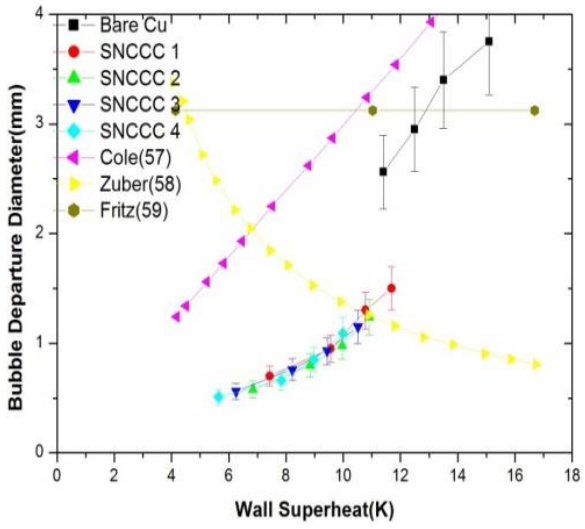

Fig. 13 D_d (departure dia. of bubble) Vs wall superheat

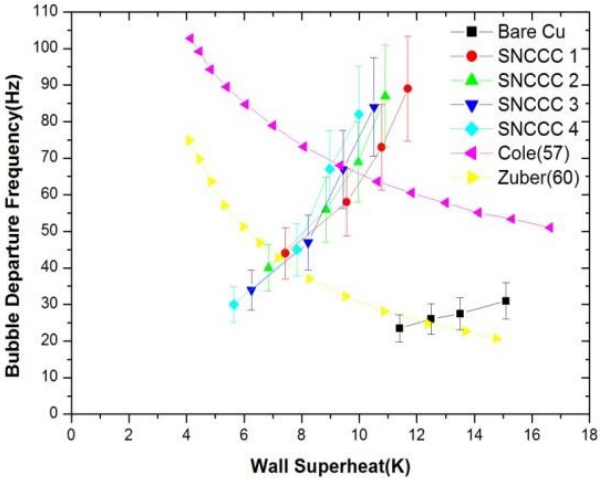

Fig. 14 D_f fluctuation with average wall superheat *(ΔT)*

buoyancy, which serves as the main lifting force, is balanced by the surface tension force (σ). After this, the bubble continued to grow and eventually managed to readily escape the heated boiling surface. The bubbles are extremely rounded in shape and quickly separate from the superhydrophilic surface. The bubble diameters on all superhydrophilic surfaces become smaller as wettability increases for a constant heat flux (Hsu & Chen, 2012). Figure 13 illustrates the D_d fluctuation with wall superheat. All SNCCC surfaces exhibit an increase in bubble size as the wall superheat increases. Figure 11 demonstrates how D_d is reliant on the nucleation site. When there are many vapour bubbles that are removed from the surface quickly, the boiling performance rises. On the superhydrophilic SNCCC surface, huge no of little and round shape bubbles can be seen to form continuously. The SNCCC surface is substantially faster at releasing bubbles in comparison with the basic Cu surface**.** On superhydrophilic surfaces, the bubble size and the time of bubble release are smaller, which contributes to a rise in the frequency of bubble occurrence. Due to this, the boiling performance is enhanced by the SNCCC surfaces.

The bubble departure diameter has been calculated analytically based on a number of variables using a variety of models that have been created to far. One of the popular models is the Fritz model (Fritz, 1935). Equation 11's relationship between the forces of buoyancy and surface tension was taken into account by Fritz's model.

$$D_d = 0.0208\theta\sqrt{\frac{\sigma}{g(\rho_l-\rho_v)}} \tag{11}$$

Cole (1967) modifies the Fritz model by incorporating wall superheat. In Cole correlation, a new constant is added in place of the CA (contact angle) term. Equation 12 provides the correlation of Cole.

$$D_d = 0.04Ja^*\sqrt{\frac{\sigma}{g(\rho_l-\rho_v)}} \tag{12}$$

Where, energy factor is defined by Ja^*.

Another well-known correlation is the correlation of Zuber (Zuber 1959), which is employed to estimate D_d and is given by equation 13.

$$D_d = \frac{C_p\rho_l(T_w-T_{sat})}{h_{lv}\rho_v}\hat{A}.\frac{\lambda(T_w-T_{sat})}{q} \tag{13}$$

In the above equation, vaporization latent heat is h_{lv} and the heat capacity is C_p.

Figure 13 compares different models' predictions with practical measurements of D_d. Figure 13 illustrates how the D_d of the SNCCC surfaces similarly reflects the pattern identified by the visualization and with Cole correlation, bare Cu surface's D_d is obviously quite reliable

3.4.3 Bubble Emission Frequency

By computing the amount of bubbles escaped from a specific bubble site per unit time, the emission frequency of the bubble (D_f) is identified. A visual depiction (Fig. 11) is used to compute the D_f for all heated surfaces and Fig. 14 illustrates how it changes as wall superheat *(ΔT)* increases. As a result of the production of porous nano-composite coating, the SNCCC surfaces' porosity and roughness are increased in contrast to the uncoated copper surface. This porous coating's porosity encourages the formation of bubbles during boiling. The SNCCC surfaces contain huge amount of micro-pits and cavities on porous nano-coated surfaces, which trap the vapour and provide a large number of bubble sites for bubble generation. The cavities and micro-pits present on the nano-coated porous (SNCCC) surfaces which capture the vapour and produce a huge number of bubble sites for bubble production. The SNCCC surfaces' increase in bubble sites results in an increase in the D_f in comparison with the uncoated copper surfaces. Figure14 displays that, at lower ΔT zone, improvements in surface wettability lead to a decrease in the frequency of bubble emissions (D_f), as extremely wetted surfaces have longer waiting and growth times for bubbles. However, as ΔT increases, the D_f of highly wetted coated surfaces enhances significantly relative to low wetted coated surfaces. This occurs because more bubbles are produced at the region of high heat flux because more bubble sites become active there, which were dormant during the lower heat flux area in the case of excessively

wet surfaces. Additionally, the liquid from the adjacent sides immediately flows to the heated area of the surface due to high capillary wicking of the superhydrophilic surfaces when the bubble is released from the boiling surface. Because of this, the D_f rises, which outcomes in further improvement in CHF. The greater thermal conductivity of the GNP causes a rise in the internal heat conduction rate of the nano-coating. This enhancement in internal conduction rate of heat increases the nucleation process, reduces the growth force of bubble, reduces diameter of bubble, and increases D_f compared to bare copper, improving the CHF (Mao et al., 2020). Although the D_f on highly wetted surfaces is lower than on less wetted surfaces, but by allowing the majority of heat to travel through the thinner liquid micro-layer that forms beneath the bubble on superhydrophilic surfaces, highly wetted surface (superhydrophilic) enhances the BHTC.

For estimating bubble emission frequency, the widely used two correlations are the Zuber correlation (Zuber, 1963) and the Cole correlation (Cole, 1967). In Fig. 14, the results of these two correlations are shown with the D_f of basic Cu surface and SNCCC surfaces.

Correlation of Cole is:

$$f = \frac{114.2}{D_b^{0.5}} \tag{14}$$

Zuber correlation:

$$D_b f = 0.59 \left[\frac{\sigma g(\rho_l - \rho_v)}{\rho_l^2}\right]^{0.25} \tag{15}$$

3.5 Assessment of Current Experimental Result with Earlier Published Literatures

A comparison is done between the pool boiling curve of SNCCC4 surface (most effective) and the previous literatures to further understand the findings of the current study. A comparison of the current results with some previously published data is depicted by Fig. 15 (Betz et al.,2010; Kwark et al., 2010; Patil et al., 2014; Shi et al., 2015; Das et al., 2016; Dharmendra et al., 2016; Das et al.,2017b; Gupta & Misra, 2018). Figure 15 makes it clear that in the current work, ONB of SNCCC 4 starts at a comparatively lower ΔT, and this trend is also present in earlier literature that has been published. The current SNCCC4 surface's ONB is lower even when compared to several published literatures. Figure 15 displays very clearly how the GNP/Ni-TiO_2 nanocomposite coating significantly benefits boiling surface engineering. The GNP/Ni-TiO_2 nanocomposite coated surface (SNCCC 4) produced in the present work is hence suitable for high heat flux situations.

3.6 Hydrothermal Stability Analysis

To do the stability analysis of the fabricated surface (SNCCC 4) in hydrothermal environment, the boiling performance of SNCCC 4 surface is tested for three times in succession, separated by a 24-hour period. The fabricated surface's boiling curve for three consecutive runs are shown in Fig. 16. The figure makes it obvious that the boiling curve for each run exhibits the same pattern. On repeated tests, however, the curve of boiling

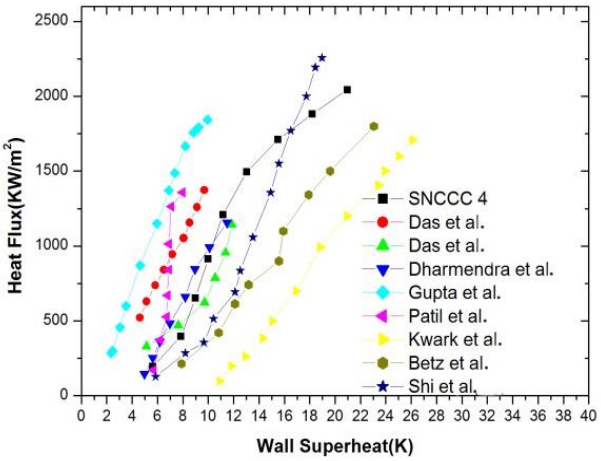

Fig. 15 Comparison between the current study (SNCCC-4) and the previous published results

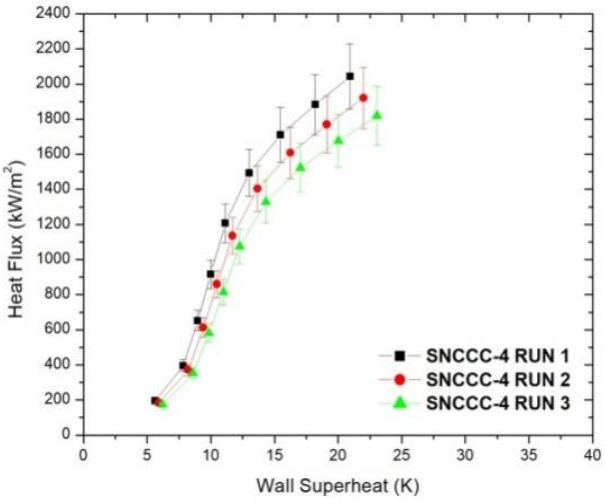

Fig. 16 Boiling curves of the stability analysis of SNCCC4

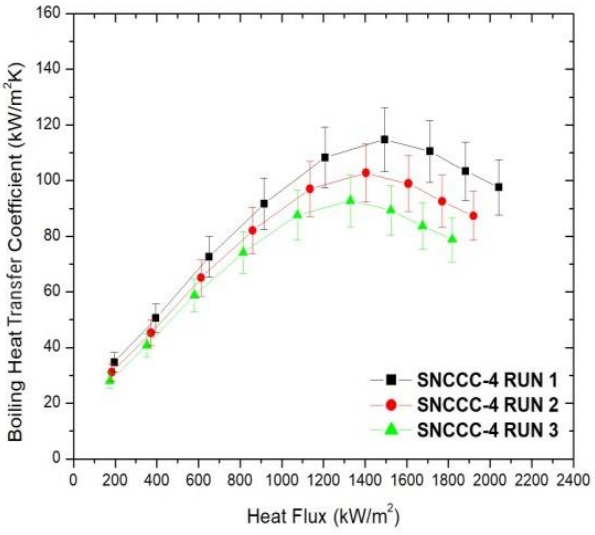

Fig. 17 BHTC vs Heat flux for the stability analysis of SNCCC4

moved slightly to the right. This suggests the enhancement in wall superheat. It is noticed that, there is a little amount of reduction in CHF on three consecutive runs for the boiling performance of the surface SNCCC4. This slight amount of reduction in CHF is due to the re-crystalline and rearrangement of the nano-composite microstructures and also due to reduction in surface wettability after consecutive runs for the boiling performance. It is also noticed that, there is small amount of reduction in BHTC during the repeated test runs of the SNCCC4 surface. This decrease in BHTC is ascribed to the rise in wall superheat during repeated test run. Therefore, the fabricated GNP/Ni-TiO_2nanocomposite coated copper surface can be regarded as stable and resistant with excellent performance of heat transfer.

4. CONCLUSION

An experimental investigation of nucleate pool boiling is carried out on GNP/Ni-TiO_2 nanocomposite coated Cu surfaces in the present study. The study of the bubble characteristics is also conducted for these coated surfaces. The remarkable following findings are enlisted based on the experimental analysis and results.

- Hybrid method is used for the production of the Cu surfaces covered with GNP/Ni-TiO_2 nanocomposite coating.
- The SNCCC surface is examined for porosity, roughness, wettability, EDX, and other characteristics, and it exhibits qualities that are appropriate for enhancing boiling heat transfer.
- CHF and BHTC augmentation is obtained for the SNCCC surfaces in comparison with the uncoated Cu surface. Highest value of critical heat flux (CHF) & BHTC are achieved 2043 kW/m^2 and 97.52 kW/m^2K, respectively, for the SNCCC 4 with CA 12^0.
- The outcomes demonstrate that CHF and BHTC are enhanced for superhydrophilic surfaces by enhancing wettability, which means by reducing the CA.
- The visualisation makes clear that the SNCCC surfaces' N_a is higher than the Cu surface without a coating.
- Compare to the uncoated Cu surface, the SNCCC surfaces exhibit a prior commencement of ONB.
- On coated (SNCCC) surfaces, small and spherical shape bubbles have been observed to develop.
- Nanocomposite-coated surfaces exhibit greater bubble emission frequencies than bare copper surface. This increased D_f aids in improving the performance of heat transfer while boiling.
- The SNCCC surfaces, fabricated by using hybrid method can be used in engineering applications involving high heat flux.

ACKNOWLEDGEMENTS

The CIC Tripura University and NIT Arunachal Pradesh are gratefully acknowledged by the authors for their contributions of FESEM images and experimental effort, respectively.

CONFLICT OF INTEREST

The authors have acknowledged no clash of interest.

AUTHORS CONTRIBUTION

Biresh Shil: Conceptualization, Methodology, Validation, Investigation, Visualization, Writing- Original draft preparation. **Dipak Sen**: Conceptualization, Supervision, Writing- Reviewing and Editing. **Ajoy Kumar Das**: Supervision, Writing- Reviewing. **Pulak Sen**: Formal analysis, Writing- Reviewing and Editing. **Sanjib Kalita**: Writing- Reviewing and Editing.

REFERENCES

Ahn, H. S., Sinha, N., Zhang, M., Banerjee, D., Fang, S., & Baughman, R. H. (2006). Pool boiling experiments on multiwalled carbon nanotube (MWCNT) forests. *Journal of Heat Transfer*, *128*(12), 1335-1342. https://doi.org/10.1115/1.2349511

Al-Chaabawi, M. J. H., Abdollahi, A., & Najafi, M. (2023). Pool boiling heat flux of ammonia refrigerant in the presence of iron oxide nanoparticles: A molecular dynamics approach. *Engineering Analysis with Boundary Elements*, *151*, 387-393. https://doi.org/10.1016/j.enganabound.2023.03.012

Alvariño, P. F., Simón, M. L. S., Guzella, M. S., Paz, J. M. A., Jabardo, J. M. S., & Gómez, L. C. (2019). Experimental investigation of the CHF of HFE-7100 under pool boiling conditions on differently roughened surfaces. *International Journal of Heat and Mass Transfer*, *139*, 269–279. https://doi.org/10.1016/j.ijheatmasstransfer.2019.04.142

Arenales, M. R. M., Kumar, S. C. S., Kuo, L. S., & Chen, P. H. (2020). Surface roughness variation effects on copper tubes in pool boiling of water. *International Journal of Heat and Mass Transfer*, *151*, 119399. https://doi.org/10.1016/j.ijheatmasstransfer.2020.119399

Benjamin, R. J., & Balakrishnan, A. R. (1997). Nucleation site density in pool boiling of saturated pure liquids: effect of surface microroughness and surface and liquid physical properties. *Experimental Thermal and Fluid Science*, *15*, 32–42. https://doi.org/10.1016/S0894-1777(96)00168-9

Betz, A. R., Xu, J., Qiu, H., & Attinger, D. (2010). Do surfaces with mixed hydrophilic and hydrophobic areas enhance pool boiling?. *Applied Physics Letters*, *97*, 141909. https://doi.org/10.1063/1.3485057

Chu, K. H., Enright, R., & Wang, E. N. (2012). Structured

surfaces for enhanced pool boiling heat transfer. *Applied Physics Letters*, *100*, 241603. https://doi.org/10.1063/1.4724190

Chuang, T. J., Chang, Y. H., & Ferng, Y. M. (2019). Investigating effects of heating orientations on nucleate boiling heat transfer, bubble dynamics, and wall heat flux partition boiling model for pool boiling. *Applied Thermal Engineering*, *163*, 114358. https://doi.org/10.1016/j.applthermaleng.2019.114358u

Cole, R. (1967). Bubble frequencies and departure volumes at subatmospheric pressures. *AIChE Journal*, *13*, 779–783. https://doi.org/10.1002/aic.690130434

Cooke, D., & Kandlikar, S. G. (2012). Effect of open microchannel geometry on pool boiling enhancement. *International Journal of Heat and Mass Transfer, 55*(4), 1004–1013. https://doi.org/10.1016/j.ijheatmasstransfer.2011.10.010

Dai, B., Qi, H., Liu, S., Zhong, Z., Li, H., Song, M., Ma, M., & Sun, Z. (2019). Environmental and economical analyses of transcritical CO_2 heat pump combined with direct dedicated mechanical subcooling (DMS) for space heating in China. *Energy Conversion and Management,198*, 111317. https://doi.org/10.1016/j.enconman.2019.01.119

Das, A. K., Das, P. K., & Saha, P. (2007). Nucleate boiling of water from plain and structured surfaces. *Experimental Thermal and Fluid Science*, *31*(8), 967–977. https://doi.org/10.1016/j.expthermflusci.2006.10.006

Das, S., Kumar, D. S., & Bhaumik, S. (2016). Experimental study of nucleate pool boiling heat transfer of water on silicon oxide nanoparticle coated copper heating surface. *Applied Thermal Engineering*, *96*, 555–567. https://doi.org/10.1016/j.applthermaleng.2015.11.117

Das, S., Saha, B., & Bhaumik, S. (2017a). Experimental study of nucleate pool boiling heat transfer of water by surface functionalization with crystalline TiO2 nanostructure. *Applied Thermal Engineering*, *113*, 1345–1357. https://doi.org/10.1016/j.applthermaleng.2016.11.135

Das, S., Saha, B., & Bhaumik, S. (2017b). Experimental study of nucleate pool boiling heat transfer of water by surface functionalization with SiO2 nanostructure. *Experimental Thermal and Fluid Science*, *81*, 454–465. https://doi.org/10.1016/j.expthermflusci.2016.09.009

Dharmendra, M., Suresh, S., Kumar, C. S. S., & Yang, Q. (2016). Pool boiling heat transfer enhancement using vertically aligned carbon nanotube coatings on a copper substrate. *Applied Thermal Engineering*, *99*, 61–71. https://doi.org/10.1016/j.applthermaleng.2015.12.081

Fang, X., & Dong, A. (2016). A comparative study of correlations of critical heat flux of pool boiling. *Journal of Nuclear Science and Technology*, *54*, 1-12. https://doi.org/10.1080/00223131.2016.1209138

Fawzy, M. H., Ashour, M. M., & Halim, A. M. A. E. (1996). Effect of some operating variables on the characteristics of electrodeposited Ni-α-Al2O3 and Ni-TiO2 composites. *Transactions of the IMF*, *74*(2), 72-77. https://doi.org/10.1080/00202967.1996.11871099

Fritz, W. (1935). Berechnung des maximale volume von dampfblasen. *Physikalische Zeitschrift, 36*, 379-384.

Gheitaghy, A. M., Saffari, H., & Mohebb, M. (2016). Investigation pool boiling heat transfer in U-shaped mesochannel with electrodeposited porous coating. *Experimental Thermal and Fluid Science*, *76*, 87–97. https://doi.org/10.1016/j.expthermflusci.2016.03.011

Gheitaghy, A. M., Saffari, H., & Zhang, G. Q. (2018). Effect of nanostructured microporous surfaces on pool boiling augmentation. *Heat Transfer Engineering*, *40*, 762-771. https://doi.org/10.1080/01457632.2018.1442310

Gupta, S. K., & Misra, R. D. (2018). Experimental study of pool boiling heat transfer on copper surfaces with Cu-Al2O3 nanocomposite coatings. *International Communications in Heat and Mass Transfer*, *97*, 47–55. https://doi.org/10.1016/j.icheatmasstransfer.2018.07.004

Gupta, S. K., & Misra, R. D. (2019). Effect of two-step electrodeposited Cu–TiO2 nanocomposite coating on pool boiling heat transfer performance. *Journal of Thermal Analysis and Calorimetry*, *136*, 1781–1793. https://doi.org/10.1007/s10973-018-7805-7

Hsu, C. C., & Chen, P. H. (2012). Surface wettability effects on critical heat flux of boiling heat transfer using nanoparticle coatings. *International Journal of Heat and Mass Transfer*, *55*, 3713–3719. https://doi.org/10.1016/j.ijheatmasstransfer.2012.03.003

Hu, Y., Li, H., He, Y., Liu, Z., & Zhao, Y. (2017). Effect of nanoparticle size and concentration on boiling performance of SiO2 nanofluid. *International Journal of Heat and Mass Transfer*, *107*, 820–828. https://doi.org/10.1016/j.ijheatmasstransfer.2016.11.090

Huang, C. K., Lee, C. W., & Wang, C. K. (2011). Boiling enhancement by TiO2 nanoparticle deposition. *International Journal of Heat and Mass Transfer*, *54*, 4895–4903. https://doi.org/10.1016/j.ijheatmasstransfer.2011.07.001

Jun, S., Kim, J., You, S. M., & Kim, H. Y. (2016). Effect of heater orientation on pool boiling heat transfer from sintered copper microporous coating in saturated water. *International Journal of Heat and*

Mass Transfer, *103*, 277–284. https://doi.org/10.1016/j.ijheatmasstransfer.2016.07.030

Jun, S., Ray, S. S., & Yarin, A. L. (2013). Pool boiling on nano-textured surfaces. *International Journal of Heat and Mass Transfer*, *62*, 99–111. https://doi.org/10.1016/j.ijheatmasstransfer.2013.02.046

Kim, J. S., Girard, A., Jun, S., Lee, J., & You, S. M. (2018). Effect of surface roughness on pool boiling heat transfer of water on hydrophobic surfaces. *International Journal of Heat and Mass Transfer*, *118*, 802–811. https://doi.org/10.1016/j.ijheatmasstransfer.2017.10.124

Kim, J., Seongchul, J., Laksnarain, R. & You, S. M. (2016). Effect of surface roughness on pool boiling heat transfer at a heated surface having moderate wettability. *International Journal of Heatand Mass Transfer*, *101*, 992–1002. https://doi.org/10.1016/j.ijheatmasstransfer.2016.05.067

Kim, S. J., Bang, I. C., Buongiorno, J., & Hu, L. W. (2007). Surface wettability change during pool boiling of nanofluids and, its effect on critical heat flux. *International Journal of Heat and Mass Transfer*, *50*, 4105–4116. https://doi.org/10.1016/j.ijheatmasstransfer.2007.02.002

Kocamustafaogullari, G., & Ishii, M. (1983). Aireinterfacialeetdensite de sites de nucleation dans les systemes en ebullition. *International Journal of Heat and Mass Transfer*, *26*, 1377–1387. https://doi.org/10.1016/S0017-9310(83)80069-6

Kwark, S. M., Kumar, R., Moreno, G., Yoo, J., & You, S. M. (2010). Pool boiling characteristics of low concentration nanofluids. *International Journal of Heat and Mass Transfer*, *53*, 972–981. https://doi.org/10.1016/j.ijheatmasstransfer.2009.11.018

Lu, M. C., Chen, R., Srinivasan, V., Carey, V. P., & Majumdar, A. (2011). Critical heat flux of pool boiling on Si nanowire array-coated surfaces. *International Journal of Heat and Mass Transfer*, *54*, 5359–5367. https://doi.org/10.1016/j.ijheatmasstransfer.2011.08.007

Mao, L., Zhou, W., Hu, X., Yu, H., Zhang, G., Zhang, L., & Fu, R. (2020). Pool boiling performance and bubble dynamics on graphene oxide nanocoating surface. *International Journal of Thermal Sciences*, *147*, 106154. https://doi.org/10.1016/j.ijthermalsci.2019.106154

Mogra, A., Pandey, P. K., & Gupta, K. K. (2021). Influence of surface wettability and selection of coating material for enhancement of heat transfer performance. *Materials Today: Proceedings*, *44*, 4433-4438. https://doi.org/10.1016/j.matpr.2020.10.595

Mohammadi, N., Fadda, D., Choi, C. K., Lee, J., & You, S. M. (2018). Effects of surface wettability on pool boiling of water using super-polished silicon surfaces. *International Journal of Heat and Mass Transfer*, *127*, 1128–1137. https://doi.org/10.1016/j.ijheatmasstransfer.2018.07.122

Mori, S., & Okuyama, K. (2009). Enhancement of the critical heat flux in saturated pool boiling using honeycomb porous media. *International Journal of Multiphase Flow*, *35* (10), 946–951. https://doi.org/10.1016/j.ijmultiphaseflow.2009.05.003

Namaraa, R. J. M., Luptona, T. L., Lupoia, R., & Robinson, A. J. (2019). Enhanced nucleate pool boiling on copper-diamond textured surfaces. *Applied Thermal Engineering*, *162*, 114145. https://doi.org/10.1016/j.applthermaleng.2019.114145

Nikolic, N. D. (2010). Fundamental aspects of copper electro-deposition in the hydrogen co-deposition range. *Zaštita Materijala, 51*, 197-203. https://cer.ihtm.bg.ac.rs/handle/123456789/725

Park, S. D., Lee, S. W., Kang, S., Kim, S. M., & Bang, I. C. (2012). Pool boiling CHF enhancement by graphene-oxide nanofluid under nuclear coolant chemical environments. *Nuclear Engineering and Design*, *252*, 184–191. https://doi.org/10.1016/j.nucengdes.2012.07.016

Patil, C. M., Santhanam, K. S. V., Kandlikar, S. G. (2014). Development of a two-step electro-deposition process for enhancing pool boiling. *International Journal of Heat and Mass Transfer*, *79*, 989–1001. https://doi.org/10.1016/j.ijheatmasstransfer.2014.08.062

Phan, H. T., Caney, N., Marty, P., Colasson, S., & Gavillet, J. (2009). Surface wettability control by nanocoating: The effects on pool boiling heat transfer and nucleation mechanism. *International Journal of Heat and Mass Transfer*, *52*, 5459–5471. https://doi.org/10.1016/j.ijheatmasstransfer.2009.06.032

Rishi, A. M., Gupta, A., & Kandlikar, S. G. (2018). Improving aging performance of electrodeposited copper coatings during pool boiling. *Applied Thermal Engineering*, *140*, 406–414. https://doi.org/10.1016/j.applthermaleng.2018.05.061

Rishi, A. M., Kandlikar, S. G., & Gupta, A. (2019). Improved wettability of graphene nanoplatelets (GNP)/copper porous coatings for dramatic improvements in pool boiling heat transfer. *International Journal of Heat and Mass Transfer*, *132*, 462–472. https://doi.org/10.1016/j.ijheatmasstransfer.2018.11.169

Rohsenow, W. M. (1952). A method of correlating heat

transfer data for surface boiling of liquids. *Trans. ASME*, *74*(6), 969-975. https://doi.org/10.1115/1.4015984

Saeidi, D., & Alemrajabi, A. A. (2013). Experimental investigation of pool boiling heat transfer and critical heat flux of nanostructured surfaces. *International Journal of Heat and Mass Transfer*, *60*, 440–449. https://doi.org/10.1016/j.ijheatmasstransfer.2013.01.016

Saelim, N., Magaraphan, R., & Sreethawong, T. (2011). Preparation of sol–gel TiO2/purified Na-bentonite composites and their photovoltaic application for natural dye-sensitized solar cells. *Energy Conversion and Management*, *52*, 815–2818. https://doi.org/10.1016/j.enconman.2011.02.016

Seo, H., Chu, J. H., Kwonb, S. Y., & Bang, I. C. (2015). Pool boiling CHF of reduced graphene oxide, graphene, and SiC-coated surfaces under highly wettable FC-72. *International Journal of Heat and Mass Transfer*, *82*, 490–502. https://doi.org/10.1016/j.ijheatmasstransfer.2014.11.019

Shah, Y., Kim, H. G., Choi, W. W., & Kim, S. M. (2023). Experimental pool boiling study on novel multistage cross-flow porous structure using FC-72 for high-heat-flux electronic applications. *International Journal of Heat and Mass Transfer*, *213*, 124270. https://doi.org/10.1016/j.ijheatmasstransfer.2023.124270

Shi, B., Wang, Y. B., & Chen, K. (2015). Pool boiling heat transfer enhancement with copper nanowire arrays. *Applied Thermal Engineering*, *75*, 115-121. https://doi.org/10.1016/j.applthermaleng.2014.09.040

Shi, J., Jia, X., Feng, D., Chen, Z., & Dang, C. (2020). Wettability effect on pool boiling heat transfer using a multiscale copper foam surface. *International Journal of Heat and Mass Transfer*, *146*, 118726. https://doi.org/10.1016/j.ijheatmasstransfer.2019.118726

Tang, Y., Tang, B., Li, Q., Qing, J., Lu, L., & Chen, K. (2013). Pool-boiling enhancement by novel metallic nanoporous surface. *Experimental Thermal and Fluid Science*, *44*, 194–198. https://doi.org/10.1016/j.expthermflusci.2012.06.008

Tey, E., Hashim, M., & Ismail, I. (2015). Characterization of Cu-Al2O3 and Ni-Al2O3 nanocomposites electrodeposited on copper substrate. *Materials Science Forum*, *846*, 471-478. http://dx.doi.org/10.4028/www.scientific.net/MSF.846.471

Ujereh, S., Fisher, T., & Mudawar, I. (2007). Effects of carbon nanotube arrays on nucleate pool boiling. *International Journal of Heat and Mass Transfer*, *50*, 4023–4038. https://doi.org/10.1016/j.ijheatmasstransfer.2007.01.030

Vemuri, S., & Kim, K. J. (2005). Pool boiling of saturated FC-72 on nano-porous surface. *International Communications in Heat and Mass Transfer*, *32*, 27–31. https://doi.org/10.1016/j.icheatmasstransfer.2004.03.020

Wang, C. H., & Dhir, V. K. (1993). Effect of surface wettability on active nucleation site density during pool boiling of water on a vertical surface. *Journal of Heat Transfer*, *115*(3), 659-669. https://doi.org/10.1115/1.2910737

Wang, C. Y., JI, W. T., Zhao, C. Y., Chen, L., & Qua, W. (2023a). Experimental determination of the role of roughness and wettability on pool-boiling heat transfer of refrigerant. *International Journal of Refrigeration.* https://doi.org/10.1016/j.ijrefrig.2023.06.014

Wang, Y. Q., Luo, J. L., Heng, Y., Mo, D. C., & Lyu, S. S. (2018). Wettability modification to further enhance the pool boiling performance of the micro nano bi-porous copper surface structure. *International Journal of Heat and Mass Transfer*, *119*, 333–342. https://doi.org/10.1016/j.ijheatmasstransfer.2017.11.080

Wang, Y., Wu, G., Xu, J., Chen, R., & Wang, H. (2023b). Effects of geometric arrangement on pool boiling heat exchange in the tubular bundle. *Nuclear Engineering and Design*, *402*, 112110. https://doi.org/10.1016/j.nucengdes.2022.112110

Yeom, H., Sridharan, K., & Corradini, M. (2015). Bubble dynamics in pool boiling on nanoparticle-coated surfaces. *Heat Transfer Engineering*, *36*(12), 1013–1027. https://doi.org/10.1080/01457632.2015.979116

Yim, K., Lee, J., Naccarato, B., & Kim, K. J. (2019). Surface wettability effect on nucleate pool boiling heat transfer with titanium oxide (TiO2) coated heating surface. *International Journal of Heat and Mass Transfer*, *133*, 352–358. https://doi.org/10.1016/j.ijheatmasstransfer.2018.12.075

Zuber, N. (1959). *Hydrodynamic aspects of boiling heat transfer.* [thesis, United States Atomic Energy Commission], Technical Information Service. https://doi.org/10.2172/4175511

Zuber, N. (1963). Nucleate boiling. The region of isolated bubbles and the similarity with natural convection. *International Journal of Heat and Mass Transfer*, *53*-78. https://doi.org/10.1016/0017-9310(63)90029-2